Research Article

Shreyas R. Hole and Agam Das Goswami*

Design of an efficient MPPT optimization model via accurate shadow detection for solar photovoltaic

https://doi.org/10.1515/ehs-2022-0151
Received November 19, 2022; accepted January 14, 2023;
published online March 24, 2023

Abstract: The output of Solar Panels is directly dependent on the intensity of direct Sunlight that is incident on the panels. But this efficiency reduces due to shadow effects for rooftop-mounted panels. These shadows can come from other solar panels, nearby buildings, or high-rise structures. It is possible to optimize Maximum Power Point Tracker (MPPT) controllers, which draw the most power possible from PV modules by forcing them to function at the most efficient voltage to increase the output of solar panels even while they are in the shade. Thus, the MPPT analyses the output of the PV module, compares it to the voltage of the battery, and determines the best power the PV module can provide to charge the battery. It then converts that power to the optimum voltage to allow the battery to receive the maximum level of currents. Additionally, it can power a DC load linked directly to the battery. Existing shadow detection and MPPT control models are highly complex, which increases their computational requirements, thereby reducing the operating efficiency of the solar panels. This text discusses a novel Saliency Map-based low-complexity shadow detection model for Solar panels to overcome this issue. The proposed model initially extracts saliency maps from connected Solar panel configurations and evaluates the background for the presence of shadows. Based on the intensity shadows, the model tunes MPPT parameters for optimal voltage & current outputs. Due to this, the model can maximize Solar panel output by over 8.5%, even under shadows, making it useful for various real-time use cases.

Keywords: current; MPPT; saliency; shadow; solar panel; voltages.

***Corresponding author: Dr Agam Das Goswami**, VIT-AP University, Amaravati, India, E-mail: agam.goswami@vitap.ac.in. https://orcid.org/0000-0002-3341-0597
Shreyas R. Hole, VIT-AP University, Amaravati, India, E-mail: rajendra.20phd7078@vitap.ac.in. https://orcid.org/0000-0002-1432-2196

Introduction

Computer vision applications risk making an erroneous determination regarding the nature of the objects or information contained in a scene when shadows are present. Because they do not belong in the foreground or the background, locating and removing them is essential to any analysis that can be relied upon. It's possible that identifying shadows will be complex due to the diverse item types and colors present in the scene, as well as the inconsistent lighting in the image. It is challenging to create a general model to recognize different types of shadows in different environments, such as indoors and outdoors, because of the obstacles listed above. This is because the manifestation of these issues can take on many different forms, depending on the particulars. As a result, they are having difficulty developing a model that can distinguish between various kinds of shadows in both indoor and outdoor settings. To address this problem, several different shadow detection systems have been developed. Photos contain information about the RGB color space and the pixel intensity, both of which can be used to locate regions significantly darker than their immediate surroundings. It is possible to extract information on chrominance and illuminance from the original image by converting it to a different color space. This paves the way for more advanced techniques. Objects can also be categorized according to photographic qualities such as lighting and texture, and additional techniques exist.

In addition, the techniques make use of light and reflectance or chromaticity in a variety of different permutations in an effort to differentiate shadows on multiple levels. These levels include pixel-based (Alvarado-Robles et al. 2021), edge-based (EB) (Alsaffar et al. 2021), and region-based (Bo, Fenzhen, and Yunshan 2020). In order to perform chromaticity-based shadow detection, the original image needs to be converted into a new colour space. Within this new colour space, the chrominance and luminance information must be kept distinct from one another. Chroma is represented by the H and S components of the HSV model (Campbell, Lin, and Chen 2019), while luminance is

represented by the *V* component of the model. The RGB, YUV, and HSI colour spaces, in addition to the c1c2c3 colour space (Campbell, Lin, and Chen 2019; Dong et al. 2020; Fang et al. 2019). Compared to the RGB model, these colour models have a number of advantages, the most notable of which is the consistency and linearity with which they display colours, which is independent of the intensity. After being converted into the LAB colour space, the image is analysed pixel by pixel to determine the presence of shadows. Shadows are denoted by pixels whose values are lower than the average of the L component (Gutierrez, Elmannai, and Elleithy 2022). This method was successful in identifying nearly all shadows that were encountered in real-world scenarios; however, it incorrectly labelled pixels with very high saturations of the colours blue, red, and green as well as black as shadows, which resulted in poor performance when detecting features that were not cast in darkness.

The method described in Hu et al. (2020) is an advancement on the previous method because it thresholds, uses the mean of the B and A components as another criterion for identifying shadows, and uses the mean of the B component as another criterion for identifying shadows. The realization that blue accounts for a significantly higher proportion of shadows than any other colour is the basis for this strategy's overall approach. Because of this, it is possible to identify blue pixels as shadows, whereas red and green pixels cannot be. Although it was significantly less successful than the method that came before it and continued to have the same flaws, it was selected as the method of choice. In Hou et al. (2021), thresholding the shaded pixels, also known as TSP, is discussed. This section uses the Tri-colour Attenuation Model to generate a ratio map (TAM). The fact that these techniques are applied at the pixel level, which results in a large number of false pixels being identified as shadows, is the primary problem that arises when trying to use them in environments that are outdoors, in which the lighting conditions can vary considerably from one location to the next. It is possible to pinpoint the locations of shadows on a given surface by comparing the texture of the surface in areas of high light to the texture of the surface in areas of low light, as was discussed in Hole and Das Goswami (2022a, 2022b). It is possible to recognize clouds in natural settings by noticing how the brightness of the image's foreground objects has been reduced. The surface of a building to be lit up for a human to be able to see a shadow that is projected onto the surface of the building. This finding led to the development of an algorithm for detecting shadows, which was subsequently incorporated into the method described in Inoue and Yamasaki (2021), Kumar and Panda (2022, 2023), and Kumar, Singh, and Panigrahi (2022). These techniques made use of light and texture in order to generate pairs of shadowed and unshaded regions (LTSUR) in the image. In Kumari, Kumar, and Panigrahi (2023), Liu et al. (2022), Liu, An, and Huang (2019), Luo et al. (2021), and Mohajerani and Saeedi (2019), which discuss the use of low complexity optimization models that can be used for multiple use cases, efficient techniques are also proposed. These models can be used for a variety of applications. The accuracy and independence of the chromaticity information provided by such systems are undeniably positive aspects of the technology, but the lengthy processing times are undeniably a drawback.

In the following paragraphs, we will go over developing a low-complexity shadow detection model for solar panels based on saliency maps. The suggested model extracts saliency maps from connected solar panel configurations and assesses the background for shadow presence (Saha, Kumar, and Panda 2022). Based on the intensity shadows, the model adjusts the MPPT parameters for the best voltage and current outputs based on the intensity shadows. The model is validated in Section 3, where its results are compared with standard shadow detection techniques. Finally, this text concludes with deployment-specific observations about the proposed model and recommends methods to improve its performance under different use cases.

Materials & methods

It was determined via the evaluation of older shadow detection models that contemporary control models are highly intricate, boosting their computational needs and reducing the operational efficiency of the solar panels. This was discovered as a result of the findings. To solve this issue, the author of this book presents a novel and simple shadow detection model for solar panels based on saliency maps. The proposed method first gathers saliency maps from connected solar panel sets and then evaluates the background to determine whether or not there is a shadow. The model considers the intensity of the shadows to make any necessary adjustments to the MPPT parameters (Siu, Kumar, and Panda 2022; Wei et al. 2019). Implementing these algorithms is limited because identifying shadows cast by solar panel installations requires context-specific strategies. These strategies must be implemented. A general-purpose object recognition model is built with the help of a structure- and colour-based saliency map model in this book. The model estimates the saliency map by applying bit-level slicing, colour space conversion, structural and colour feature extraction, feature selection, and entropy analysis. The saliency map is evaluated using several rooftops, closed-circuit television (CCTV) footage, and drone images. As a result of this evaluation, it was discovered that the recommended model is highly successful in estimating the shadows. As a result of this, the model has been used for the detection of shadow advancement stages. The progression of this process is shown in Figure 1, which displays the entropy evaluation and colour conversion. The technique starts with the frame-by-frame segmentation of the gathered input video and then moves on to the bit-level slicing of each frame (Wang et al. 2020). To construct

these slices, which each include bit-level photos for superior pixel-level interpolation, the following equation (1) is applied,

$$S_i = \bigcup_{r,c}^{N,M} \left(P_{r,c} \oplus 2^i\right) \tag{1}$$

where S_i It represents the slice pixels for ith a bit while $P_{r,c}$ is the pixel intensity of each input image pixel, and R, C represents the total number of rows and columns present in the image sets.

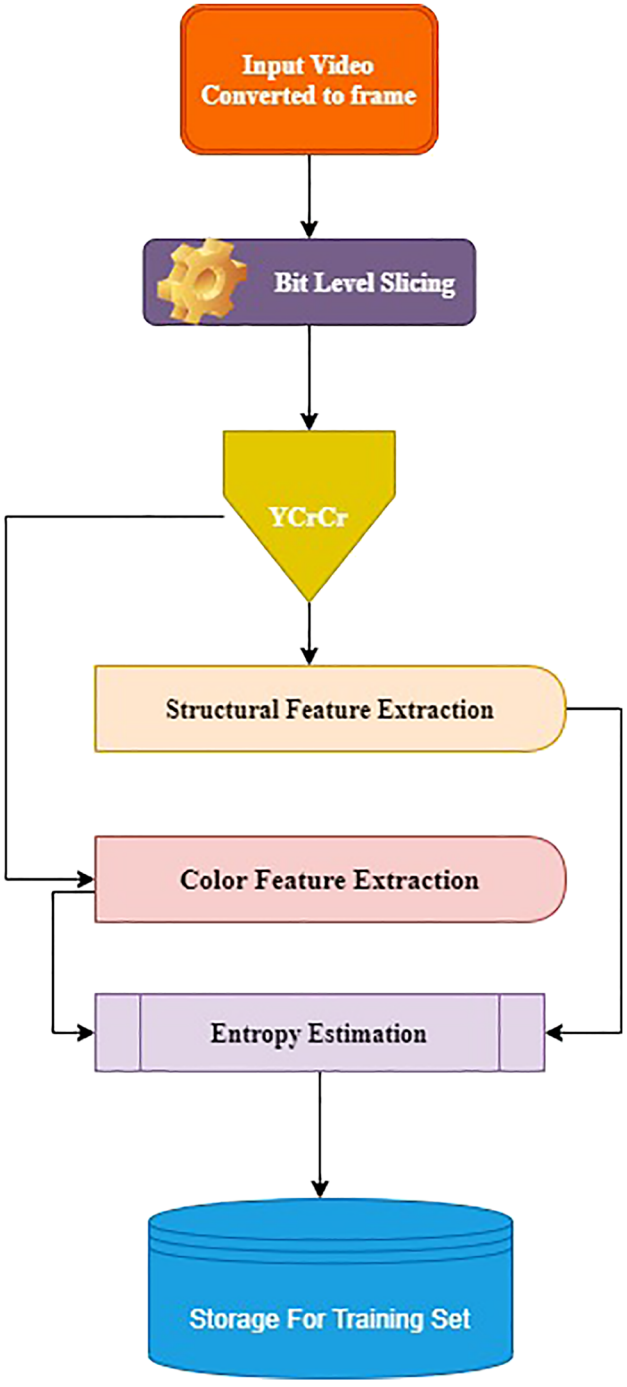

Figure 1: The overall flow of the proposed shadow detection process.

Equations (2)–(4) are used to estimate the level of approximate energy (Y), luminance levels (Cb), and levels of chrominance (Cr) of each slice based on its respective red (R), green (G), and blue (B) colour levels. All of the portions are then subjected to the YCbCr conversion. This process produces 24 separate images, each containing a unique mix of the feature levels in the original image.

$$Y = 16 + (65.481 \times R \times 128.553 \times G + 24.966 \times B) \tag{2}$$

This equation (2) is used to convert RGB image pixels into intensity levels.

$$C_b = 128 + (-37.797 \times \mathrm{R} - 74.203 \times \mathrm{G} + 112 \times B) \tag{3}$$

$$C_r = 128 + (112 \times R - 93.786 \times G - 18.214 \times B) \tag{4}$$

Estimate the average of each image via equation (5),

$$I_{\mathrm{avg_i}} = \frac{1}{N \times M} \times \sum_{r,c}^{N,M} C_i \tag{5}$$

where C_i represents the level of colour for ith a component of the image and $I_{\mathrm{avg_i}}$ is the average of given image sets. A differential bit slice value is estimated via equation (6),

$$(s_i, s_j) = \frac{1}{N \times M} \times \sum_{\mathrm{i=1}}^{N_S} I_{\mathrm{avg_i}} \times \sqrt{\sum_{r,c}^{N,M} \frac{\left(P_{i_r} - P_{j_r}\right)^2 + \left(P_{i_c} - P_{j_c}\right)^2}{\mathrm{Var}\,(s_i, s_j)}} \tag{6}$$

where $d(s_i, s_j)$ represents Euclidea instance for slice $S_{i,\ j}$; $\mathrm{Var}(s_i, s_j)$ is their variance levels, N_s are whole slices present in the image sets and P_{x_y} are the intensity of pixel levels for the image x, under the yth dimensions.

Each distance metric is given to the color and shape of feature extraction units to classify the extracted features as feature vectors to enable the units to classify the extracted features as feature vectors. Equation (7) first uses the color feature extraction and shape feature extraction units to quantize each pixel in the 0 to 128 range. This is done to reduce the number of retrieved color map values and standardize the output features.

$$P_{\mathrm{quant}=}P_{\mathrm{in}} \times \frac{128}{P_{\mathrm{max}}} \tag{7}$$

where, P_{in}, P_{quant}, *and* P_{max} are the input pixels, total quantized pixels and maximum intensity levels of output pixels? Evaluate the number of pixels needed in individual quantized image sets via equation (8), and capture their counts in output array sets.

$$\mathrm{CF_{out}} = \bigcup_{i=1}^{N_s} \sum_{r,c}^{N,M} \left|P_{r,c} == P_{\mathrm{quant}_{r,c}}\right| \tag{8}$$

where $\mathrm{CF_{out}}$ is the output colour map for all quantized pixel sets? Now identify shape levels via equation (9),

$$\mathrm{SF_{out}} = \bigcup_{(i=1)}^{(N_s)} \sum_{(r,c)}^{(N,M)} \left|\mathrm{Canny}\left(P_{(r,c)}, P_{(r,c)} + 1\right) = 1\right| \tag{9}$$

where, $\mathrm{SF_{out}}$ are output shape maps, and $\mathrm{Canny}(P_{r,c})$ applies Canny Edge detection on the image to evaluate pixel sets, where edges are present in the output images.

An entropy estimate unit is provided with a colour map and a shape map. This unit determines each bit slice's threshold, making it possible to estimate the bit-level saliency map. Equation (10) is used in the process of entropy assessment. This equation approximates the feature level and the feature level log to determine the final thresholds.

$$E_{fi} = -\sum_{r=1}^{N}\sum_{c=1}^{M} p\left(S_{r,c_i}\right) \times \log\left(p\left(\mathrm{S}_{\mathrm{r,c_i}}\right)\right) \tag{10}$$

where $p\left(F_{r,c_i}\right)$ represents the shadow probability of foreground pixels detected in the image sets.

To execute bit-level thresholding, these entropy values are employed as upper bounds for each slice of the input image. The whole silhouette map is constructed by combining the information from each of these slices. Figure 2 provides a window into some of the retrieved silhouette maps, allowing for precise extraction of the item that is going to be investigated to be carried out. Based on these results, a final shadow probability metric (SPM) is evaluated via equation (11),

$$\mathrm{SPM} = \sum_{i=1}^{N} \frac{E_{fi}}{N} \tag{11}$$

This shadow probability metric enables control signals for the MPPT unit, improving their computational efficiency levels. To perform this task, the Temperature Method is used, which outputs the maximum power point via equation (12),

$$V_{\mathrm{mpp}}\left(S\right) = V_{\mathrm{mpp}}\left(S_{\mathrm{ref}}\right) + \mathrm{SPM} \times \left(S - S_{\mathrm{ref}}\right) \tag{12}$$

where $V_{\mathrm{mpp}}(S)$ represents the output of MPPT at the current shadow level, $V_{\mathrm{mpp}}\left(S_{\mathrm{ref}}\right)$ represents output at reference shadow levels.

Due to the integration of saliency maps, the model is capable of high-efficiency shadow identification and improves MPPT-based control's efficiency for different solar deployments. The performance of this model is evaluated and compared with existing methods in the next section of this text (Wang et al. 2021).

Result analysis & comparison

The proposed model uses a combination of Saliency Maps with MPPT-based control to improve the efficiency of solar rooftop deployments. This efficiency was evaluated in terms of the accuracy of shadow detection (A), power conversion efficiency levels after shadow detection (PCE), and delay (D) needed for shadow detection under multiple season types. Based on different season types, the shadow percentage (SP) on Solar panels varied between 1% and 20%, and its performance was compared with various state-of-the-art models. The accuracy of shadow detection was evaluated via equation (13) and compared with EB (Alsaffar et al. 2021), TSP (Hou et al. 2021), and LTSUR (Inoue and Yamasaki 2021) in Table 1 as follows,

$$A = \sum_{i=1}^{N_i} \frac{\mathrm{SL}}{N_i \times \mathrm{SL_{act}}} \tag{13}$$

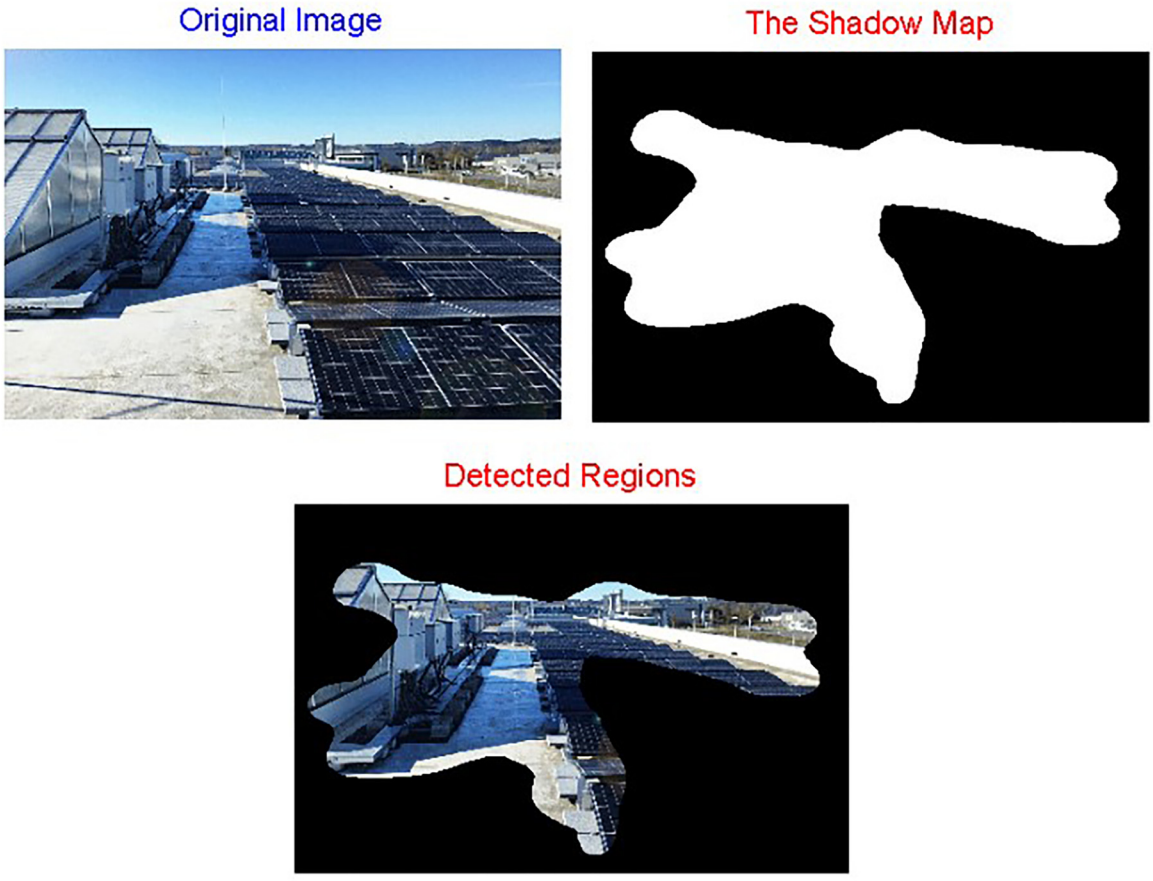

Figure 2: Extracted saliency maps from the input images.

Table 1: Accuracy of shadow detection for different models.

SP	A (%) EB (Alsaffar et al. 2021)	A (%) TSP (Hou et al. 2021)	A (%) LTSUR (Inoue and Yamasaki 2021)	A (%) proposed
1	76.50	74.30	70.50	79.04
2	76.90	74.50	70.80	79.36
3	76.95	74.90	71.80	79.88
4	77.20	75.10	72.60	80.32
5	77.30	76.20	73.90	81.21
6	77.54	76.32	74.50	81.56
7	77.73	76.76	75.36	82.09
8	77.92	77.20	76.22	82.62
9	78.11	77.64	77.08	83.15
10	78.30	78.08	77.94	83.69
11	78.49	78.52	78.80	84.22
12	78.68	78.96	79.66	84.75
13	78.87	79.40	80.52	85.28
14	79.06	79.84	81.38	85.81
15	79.25	80.28	82.24	86.35
16	79.44	80.72	83.10	86.88
17	79.63	81.16	83.96	87.41
18	79.82	81.60	84.82	87.94
19	80.01	82.04	85.68	88.48
20	80.20	82.48	86.54	89.01

Table 2: The power conversion efficiency of MPPT for different models.

SP	PCE (%) EB (Alsaffar et al. 2021)	PCE (%) TSP (Hou et al. 2021)	PCE (%) LTSUR (Inoue and Yamasaki 2021)	PCE (%) proposed
1	88.49	90.24	92.86	96.00
2	88.33	89.86	92.18	95.63
3	88.20	89.50	91.44	95.26
4	88.05	89.12	90.73	94.88
5	87.90	88.70	90.00	94.49
6	87.74	88.42	89.37	94.17
7	87.59	88.06	88.68	93.81
8	87.44	87.71	87.99	93.44
9	87.28	87.36	87.30	93.08
10	87.13	87.01	86.62	92.72
11	86.98	86.66	85.93	92.36
12	86.83	86.30	85.24	92.00
13	86.68	85.95	84.55	91.64
14	86.52	85.60	83.86	91.28
15	86.37	85.25	83.18	90.92
16	86.22	84.90	82.49	90.56
17	86.07	84.54	81.80	90.20
18	85.92	84.19	81.11	89.84
19	85.76	83.84	80.42	89.48
20	85.61	83.49	79.74	89.12

where, N_i, SL, & SL_{act} represents several images used for detection, estimated shadow levels, and actual shadow levels.

Based on this evaluation, it can be observed that the proposed model showcases 8.5% better accuracy than EB (Alsaffar et al. 2021), 6.5% better accuracy than TSP (Hou et al. 2021), and 2.9% better accuracy than LTSUR (Inoue and Yamasaki 2021) under different season types. This is due to the incorporation of Saliency Maps, which improve shadow detection performance under different season types. Similarly, the power conversion efficiency can be observed in Table 2 as follows,

Based on this evaluation, it can be observed that the proposed model showcases 3.5% better power conversion efficiency than EB (Alsaffar et al. 2021), 5.9% better power conversion efficiency than TSP (Hou et al. 2021), and 9.1% better power conversion efficiency than LTSUR (Inoue and Yamasaki 2021) under different season types. This is due to the incorporation of Saliency Maps, which improve shadow detection performance under different season types. Similarly, the delay can be observed in Table 3 as follows,

Table 3: Delay of shadow detection for different models.

SP	D (ms) EB (Alsaffar et al. 2021)	D (ms) TSP (Hou et al. 2021)	D (ms) LTSUR (Inoue and Yamasaki 2021)	D (ms) proposed
1	117.85	117.53	116.69	92.13
2	118.02	117.40	116.41	92.10
3	117.97	117.43	116.60	92.18
4	118.03	117.30	116.66	92.21
5	118.00	117.79	117.07	92.48
6	118.06	117.67	117.05	92.49
7	118.08	117.73	117.17	92.58
8	118.11	117.79	117.29	92.67
9	118.14	117.86	117.42	92.76
10	118.17	117.92	117.54	92.85
11	118.19	117.98	117.66	92.94
12	118.22	118.05	117.79	93.03
13	118.25	118.11	117.91	93.12
14	118.27	118.17	118.03	93.21
15	118.30	118.23	118.15	93.30
16	118.33	118.30	118.28	93.39
17	118.36	118.36	118.40	93.48
18	118.38	118.42	118.52	93.57
19	118.41	118.49	118.65	93.66
20	118.44	118.55	118.77	93.75

Based on this evaluation, it can be observed that the proposed model showcases 18.5% faster performance than EB (Alsaffar et al. 2021), TSP (Hou et al. 2021), and LTSUR (Inoue and Yamasaki 2021) under different season types. This is due to the incorporation of Saliency Maps, which assist in reducing the complexity of shadow detection under different season types, and makes it useful for real-time deployments. Thus, the proposed model is capable of high accuracy & low

complexity shadow detection and high conversion efficiency for different solar rooftop deployments.

Abbreviations

MPPT	maximum power point tracker
PV	photovoltaic
DC	direct current
RGB	red green blue
EB	edge-based
RGB	tri-color attenuation model
LTSUR	light and texture in order to generate pairs of shadowed and unshaded regions
HSV	hue saturation value
YUV	(*Y*) luma, or brightness, (*U*) blue projection and (*V*) red projection
HSI	hue, saturation, intensity
TSP	thresholding the shaded pixels
Y	approximate energy
Cb	luminance levels
Cr	chrominance
R	red
G	green
B	blue
A	accuracy
PCE	power conversion efficiency
D	delay
SP	shadow percentage
CCTV	closed-circuit television
CNN	convolutional ceural networks
GRU	gated recurrent unit
YCbCr	Y is the Luma component and CB and CR are the blue-difference and red-difference Chroma components

Conclusions and future scope

The proposed model combines saliency maps with MPPT-based control to identify solar rooftop shadows and improve converter efficiency via temperature-based analysis. Due to simplified entropy analysis during shadow identification, the model is useful for small-to-large-scale solar deployments. The suggested model was 8.5% more accurate than EB (Alsaffar et al. 2021), 6.5% more accurate than TSP (Hou et al. 2021), and 2.9% more accurate than LTSUR (Inoue and Yamasaki 2021). These maps contribute to improved shadow detection performance across seasons. In addition, its power conversion efficiency was 3.5% better than EB (Alsaffar et al. 2021), 5.9% better than TSP (Hou et al. 2021), and 9.1% better than LTSUR (Inoue and Yamasaki 2021). These maps contribute to improved shadow detection performance across seasons. The suggested model was 18.5% faster than EB (Alsaffar et al. 2021), TSP (Hou et al. 2021), and LTSUR (Inoue and Yamasaki 2021) in each season. Saliency Maps reduce the complexity of shadow detection across seasons and enable real-time deployments. The model can identify shadows with high precision while maintaining low complexity and high conversion efficiency across solar rooftop installations.

– **Future scope**

Future researchers can integrate deep learning models, such as Convolutional Neural Networks (CNN), Gated recurrent unit (GRU), etc., to improve computational efficiency across seasons. The model must be validated on larger deployments and can be tuned using bioinspired techniques to be useful in real-time scenarios.

Author contributions: All the authors have accepted responsibility for the entire content of this submitted manuscript and approved submission.
Research funding: None declared.
Conflict of interest statement: the authors certify that they have no affiliations with or involvement in any organization or entity with any financial interest, or non-financial interest in the subject matter or study materials discussed in this manuscript.

References

Alvarado-Robles, G., R. A. Osornio-Ríos, F. J. Solís-Muñoz, and L. A. Morales-Hernández. 2021. “An Approach for Shadow Detection in Aerial Images Based on Multi-Channel Statistics.” *IEEE Access* 9: 34240–50.

Alsaffar, M., G. Alshammari, A. Alshammari, S. Aljaloud, T. S. Almurayziq, A. A. Hamad, V. Kumar, and A. Belay. 2021. “Detection of Tuberculosis Disease Using Image Processing Technique.” *Mobile Information Systems* 2021 (2021): 1–7.

Bo, P., S. Fenzhen, and M. Yunshan. 2020. “A Cloud and Cloud Shadow Detection Method Based on Fuzzy C-Means Algorithm.” *IEEE Journal of Selected Topics in Applied Earth Observations and Remote Sensing* 13: 1714–27.

Campbell, K., C. H. Lin, and D. Chen. 2019. “Cost-Effective Error Detection Through Mersenne Modulo Shadow Datapaths.” *IEEE Transactions on Computer-Aided Design of Integrated Circuits and Systems* 38 (6): 1056–69.

Dong, Z., F. Li, J. Ying, and K. Pahlavan. 2020. “A Model-Based RF Hand Motion Detection System for Shadowing Scenarios.” *IEEE Access* 8: 115662–72.

Fang, H., Y. Wei, H. Luo, and Q. Hu. 2019. “Detection of Building Shadow in Remote Sensing Imagery of Urban Areas with Fine Spatial Resolution Based on Saturation and Near-Infrared Information.” *IEEE Journal of Selected Topics in Applied Earth Observations and Remote Sensing* 12 (8): 2695–706.

Gutierrez, A., W. Elmannai, and K. Elleithy. 2022. “Computer Vision Based Method for Shadow Detection.” *IEEE Sensors Letters* 6 (6): 23–6.

Hu, X., C. W. Fu, L. Zhu, J. Qin, and P. A. Heng. 2020. “Direction-aware Spatial Context Features for Shadow Detection and Removal.” *IEEE Transactions on Pattern Analysis and Machine Intelligence* 42 (11): 2795–808.

Hou, L., T. F. Y. Vicente, M. Hoai, and D. Samaras. 2021. "Large Scale Shadow Annotation and Detection Using Lazy Annotation and Stacked CNNs." *IEEE Transactions on Pattern Analysis and Machine Intelligence* 43 (4): 1337–51.

Hole, S. R., and A. Das Goswami. 2022a. "Quantitative Analysis of DC–DC Converter Models: A Statistical Perspective Based on Solar Photovoltaic Power Storage." *Energy Harvesting and Systems* 9 (1): 113–21.

Hole, S. R., and A. Das Goswami. 2022b. "Maintain Maximum Power Point Tracking of Photovoltaic Using SEPIC Converter," In *2022 2nd International Conference On Power Electronics and IoT Applications in Renewable Energy and its Control, PARC 2022*, 3–8.

Inoue, N., and T. Yamasaki. 2021. "Learning from Synthetic Shadows for Shadow Detection and Removal." *IEEE Transactions on Circuits and Systems for Video Technology* 31 (11): 4187–97.

Kumar, N., B. Singh, and B. K. Panigrahi. 2022. "Voltage Sensorless Based Model Predictive Control with Battery Management System: For Solar PV Powered On-Board EV Charging." *IEEE Transactions on Transportation Electrification* 1–10. https://doi.org/10.1109/TTE.2022.3213253.

Kumar, N., and S. K. Panda. 2022. "Smart High Power Charging Networks and Optimal Control Mechanism for Electric Ships." *IEEE Transactions on Industrial Informatics* 19 (2): 1476–83.

Kumar, N., and S. K. Panda. 2023. "A Multipurpose and Power Quality Improved Electric Vessels Charging Station for the Seaports." *IEEE Transactions on Industrial Informatics* 19 (3): 3254–61.

Kumari, P., N. Kumar, and B. K. Panigrahi. 2023. "A Framework of Reduced Sensor Rooftop SPV System Using Parabolic Curve Fitting MPPT Technology for Household Consumers." *IEEE Transactions on Consumer Electronics* 69 (1): 29–37.

Liu, Y., X. Zou, S. Xu, G. Xing, H. Wei, and Y. Zhang. 2022. "Real-Time Shadow Detection from Live Outdoor Videos for Augmented Reality." *IEEE Transactions on Visualization and Computer Graphics* 28 (7): 2748–63.

Luo, S., H. Li, R. Zhu, Y. Gong, and H. Shen. 2021. "ESPFNet: An Edge-Aware Spatial Pyramid Fusion Network for Salient Shadow Detection in Aerial Remote Sensing Images." *IEEE Journal of Selected Topics in Applied Earth Observations and Remote Sensing* 14: 4633–46.

Liu, Z., D. An, and X. Huang. 2019. "Moving Target Shadow Detection and Global Background Reconstruction for VideoSAR Based on Single-Frame Imagery." *IEEE Access* 7: 42418–25.

Mohajerani, S., and P. Saeedi. 2019. "Shadow Detection in Single RGB Images Using a Context Preserver Convolutional Neural Network Trained by Multiple Adversarial Examples." *IEEE Transactions on Image Processing* 28 (8): 4117–29.

Saha, J., N. Kumar, and S. K. Panda. 2022. "A Futuristic Silicon-Carbide (SiC) Based Electric-Vehicle Fast Charging/Discharging (FC/dC) Station." *IEEE Journal of Emerging and Selected Topics in Power Electronics* 1–14. https://doi.org/10.1109/JESTPE.2022.3223417.

Siu, J. Y., N. Kumar, and S. K. Panda. 2022. "Command Authentication Using Multiagent System for Attacks on the Economic Dispatch Problem," *IEEE Transactions on Industry Applications* 58 (Issue 4): 4381–93.

Wei, H., Y. Liu, G. Xing, Y. Zhang, and W. Huang. 2019. "Simulating Shadow Interactions for Outdoor Augmented Reality with RGBD Data." *IEEE Access* 7: 75292–304.

Wang, C., H. Xu, Z. Zhou, L. Deng, and M. Yang. 2020. "Shadow Detection and Removal for Illumination Consistency on the Road." *IEEE Transactions on Intelligent Vehicles* 5 (4): 534–44.

Wang, R., M. B. Alazzam, F. Alassery, A. Almulihi, and M. White. 2021. "Innovative Research of Trajectory Prediction Algorithm Based on Deep Learning in Car Network Collision Detection and Early Warning System." *Mobile Information Systems* 2021, https://doi.org/10.1155/2021/3773688.